

Periodic and quasiperiodic dynamics of optoelectronic oscillators with narrow-band time-delayed feedback

Yunjia Bao (包昀嘉), Ella Banyas, and Lucas Illing*

Department of Physics, Reed College, Portland, Oregon 97202, USA



(Received 26 July 2018; published 11 December 2018)

We present a detailed study of instabilities arising in optoelectronic oscillators with a single narrow-band time-delayed feedback loop. Such optoelectronic oscillators produce periodic solutions and may be useful as high-purity signal generators, but their nonlinear dynamics sets limits on available signal amplitudes. Starting from an integrodifferential model, we utilize approximate analytic solutions to find the stability boundaries of the periodic solutions as well as regions of multistability. Our analytical predictions are confirmed by numerical simulations and experiments.

DOI: [10.1103/PhysRevE.98.062207](https://doi.org/10.1103/PhysRevE.98.062207)

I. INTRODUCTION

Optoelectronic oscillators (OEOs) are well controlled tabletop experimental systems that are able to generate a plethora of interesting dynamical states. Research on OEOs is driven both by the need to better understand basic dynamical phenomena and by technological applications of OEOs, such as for communication [1,2], random number generation [3,4], reservoir computing [5–7] or ultrapure microwave generation [8,9], to name a few.

One widely utilized basic optoelectronic oscillator architecture is shown in Fig. 1. It consists of a nonlinearity and a time-delayed amplified and frequency-filtered feedback of the nonlinearity's optical output to its electrical input. In the particular system considered in this paper, the feedback is bandpass filtered, and the nonlinearity is provided by a Mach-Zehnder modulator, which relates the optical output to the electrical input in a \cos^2 -type fashion. The combination of the nonlinearity and the delayed feedback gives rise to a wealth of possible dynamics, such as multiple coexisting attractors and oscillatory behavior that ranges from periodic waveforms to high-dimensional chaos as well as hybrid states, such as chaotic breathers [10–14].

Although rich dynamics arise in OEOs regardless of the broadband or narrow-band nature of the feedback loop, it is nevertheless useful to distinguish these two cases, both for theoretical studies and when considering technological applications. For example, broadband OEOs are used for random number generation [3,4] and reservoir computing [5–7], whereas narrow-band OEOs are the key technology that permits efficient generation of spectrally pure microwave signals [8,9]. In the context of OEOs with an electronic bandpass filter in the feedback loop, narrow band means that the filter bandwidth $\Delta\Omega/2\pi$ is small compared to the filter's center-frequency $\Omega_0/2\pi$, whereas the opposite is true for broadband OEOs.

It has been shown [12,13] that a simple two-pole model of the bandpass filter is sufficient to reproduce the dynamics of the basic optoelectronic feedback systems shown in Fig. 1 even if the actual filter roll-off is steeper. In the two-pole model, the filter output is given by the integrodifferential equation,

$$x + \frac{1}{\Delta\Omega} \frac{dx}{dt} + \frac{\Omega_0^2}{\Delta\Omega} \int_{t_0}^t x(s) ds = \gamma \cos^2[x^{\tau_D} + \phi], \quad (1)$$

in which x is the dimensionless variable corresponding to the experimentally measured voltage, γ is the overall loop gain, τ_D is the overall loop delay, x^{τ_D} is shorthand notation for the delayed variable $x(t - \tau_D)$, and ϕ is a fixed phase that is controlled by adding a dc voltage to the Mach-Zehnder modulator input (see Refs. [12,13,15] for details).

Motivated by the technological importance of narrow-band OEOs, we present in this paper a detailed study of the periodic solutions of Eq. (1) and their stability in the narrow-band regime. Our theory does not make *a priori* assumptions about the size of the delay and is therefore applicable for a wide range of τ_D 's, including the large delay case that is relevant for high-purity microwave signal generators.

Large delays of practical OEO signal generators are often achieved by using several kilometers of optical fiber in the feedback loop [8,16]. A large delay means, in this context, that $\tau_D \gg 2\pi/\Omega_0$ or, in terms of frequency, that the fundamental delay-mode frequency $\Omega_T/(2\pi) = 1/\tau_D$ is much smaller than the filter's center frequency. Indeed, for most microwave signal generators the fundamental delay-mode frequency is smaller than the filter bandwidth, i.e., $\Omega_T \ll \Delta\Omega \ll \Omega_0$ holds.

Large delays lead to delay modes that are narrowly spaced in Fourier space and, although many of these modes fall within the bandwidth of the electronic bandpass filter, under optimal conditions, only one such mode is amplified and oscillates, resulting in the desired spectrally pure signal. Yet, as already pointed out by Chembo *et al.* [17], the narrow filter is insufficient to completely eliminate complex dynamics if the feedback gain is large. For sufficient gain, torus bifurcations (also called secondary Hopf bifurcations or Neimark-Sacker

*illing@reed.edu

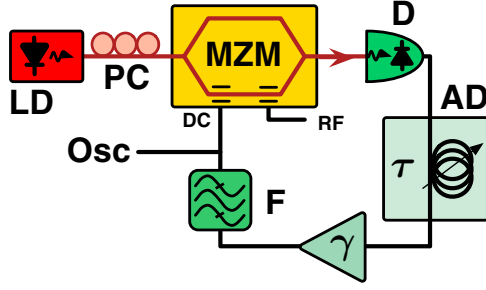


FIG. 1. Schematic of optoelectronic oscillator: LD: laser diode; PC: polarization controller; MZM: Mach-Zehnder modulator; D: photodetector; AD: adjustable delay (τ); γ : adjustable amplification; F: bandpass filter; and Osc: digital oscilloscope.

bifurcations) destabilize the periodic solutions [16,17], just as is the case for other delayed-feedback oscillators [18–21]. This bifurcation has the important implication that it sets an upper limit to the output power of an OEO signal generator.

Although the existence of an upper gain threshold for narrow-band OEOs with large delays is known [16,17], we show in this paper that the detailed picture of the periodic oscillation’s stability region is complicated because the threshold is delay dependent with several torus bifurcation curves contributing. We will pay special attention to shorter delays where the threshold value significantly differs from its value in the large delay limit. We furthermore show that stable periodic solutions coexist for certain delay values and quantify the degree to which stable periodic oscillations remain sinusoidal as their amplitudes increase.

The paper is organized as follows: A numerical analysis of the bifurcation structure of Eq. (1) is presented in Sec. II with approximate analytic solutions given in Sec. III. The experimental setup is detailed in Sec. IV, and results are discussed in Sec. V.

II. NUMERICAL BIFURCATION ANALYSIS

For ease of analysis, we rescale time with respect to the filter’s center-frequency $t \rightarrow \Omega_0 t$ and introduce the dimensionless delay $\tau = \Omega_0 \tau_D$ as well as the parameter,

$$\mu = \frac{\Delta\Omega_0}{\Omega_0}. \quad (2)$$

We note that the parameter μ is the inverse of the bandpass filter’s quality factor ($\mu = 1/Q$) and is a small parameter if the filter is narrow ($\mu = 0.22$ for our experiment). After differentiation of Eq. (1) we obtain the nonlinear delay differential equation (DDE),

$$\ddot{x} + \mu\dot{x} + x = \mu\gamma \frac{d}{dt} F[x^\tau], \quad (3)$$

where the overdot denotes the derivative with respect to rescaled time, $x^\tau = x(t - \tau)$ denotes the delayed variable, and the nonlinearity is

$$F[x^\tau] = \cos^2[x^\tau + \phi]. \quad (4)$$

We numerically find the stable regions of periodic oscillation using DDE-BIFTOOL [22,23], a software package for

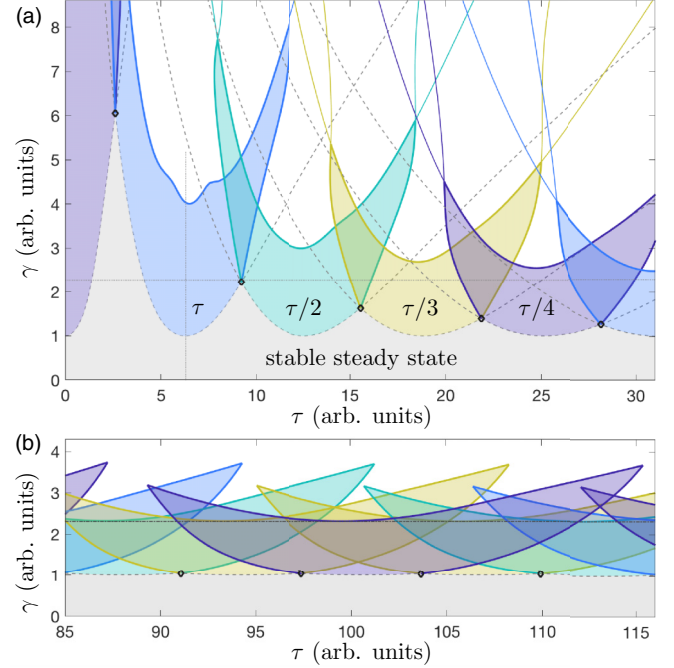


FIG. 2. Numerical bifurcation analysis in delay (τ) and feedback-gain (γ) parameter plane. Computations are performed for $\phi = -\pi/4$ (implying $\gamma = \gamma_{\text{eff}}$, see Sec. III A). (a) Short delays: stable steady state (labeled gray region), Andronov-Hopf bifurcations of steady state (dashed lines), Hopf-Hopf bifurcations of steady state (intersection of dashed lines with a subset of interest indicated by diamond symbols), stable periodic solutions (color shaded regions), torus bifurcations of periodic solutions (solid lines). Experimental measurements were taken along $\tau = 6.27$ and $\gamma = 2.28$ (dotted lines). (b) Longer delays: Only the stability regions and boundaries are shown. Asymptotic upper threshold $\gamma \approx 2.31$ (dashed-dotted line).

numerical bifurcation analysis of systems of delay differential equations. The result is shown in Fig. 2 for positive (noninverting) feedback, achieved by setting $\phi = -\pi/4$. It is seen that the $x = 0$ steady state is stable for sufficiently small feedback gain for any delay. As the gain is increased, periodic solutions are created through Andronov-Hopf bifurcations. The minimum threshold for this bifurcation is $\gamma = 1$ and occurs when the dimensionless delay τ is equal to $2\pi k$ for integer k . At these delays, which we call “integer delays,” a periodic solution with dimensionless period $T = \tau/k$ not only satisfies $x(t - \tau) = x(t)$ precisely, but also its frequency exactly matches the filter’s center frequency, implying maximum amplification per round trip. For other delays, Andronov-Hopf bifurcations occur for larger feedback gains ($\gamma > 1$), and the frequencies of periodic solutions are shifted away from the filter’s center frequency. We nevertheless can identify the different delay oscillation modes by the integer k because it still holds that $T \approx \tau/k$ ($k > 0$). Stable periodic modes with $k = 1-4$ are labeled in Fig. 2(a), and their stability regions are depicted by different colors (shades of gray).

Considering a fixed delay τ in Fig. 2(a) and increasing gain, the Andronov-Hopf bifurcation curve with minimum gain γ corresponds to a supercritical bifurcation of a stable periodic solution from the steady state, whereas Andronov-

Hopf bifurcation curves at larger gain values correspond to the creation of unstable periodic solutions. The points of intersection of two Andronov-Hopf bifurcation curves are Hopf-Hopf bifurcations of the zero steady state, and we indicate by diamonds the Hopf-Hopf points at the steady-state stability boundary. Emanating from each of the stability-boundary Hopf-Hopf points are two separate torus bifurcation curves. This is seen, for example, in Fig. 2(a) where the $k = 1$ and $k = 2$ Andronov-Hopf curves intersect in the Hopf-Hopf point at $(\tau, \gamma) \approx (9.2, 2.2)$ and two torus bifurcation curves emerge, one limiting the region of stable $k = 1$ oscillations and the other limiting the region of stable $k = 2$ oscillations.

In addition to the torus curves associated with the Hopf-Hopf points of the zero steady state, there is, for each delay mode k , an additional torus bifurcation curve that forms the upper stability boundary for that mode. For gain values in excess of the latter boundary (white regions in Fig. 2) both the zero steady state and the periodic solution are unstable.

It is seen in Fig. 2 that the upper gain threshold for stable periodic solutions strongly depends on the delay τ . The minimal threshold value is larger than 4 for short delays and decreases as the delay increases, approaching the value of 2.31 [17] for large delays. Regions of coexisting stable periodic solutions are clearly seen by the areas with overlapping colors (shades of gray).

Figure 2(b) shows the stability regions for slightly larger values of delay. It is seen that relevant features of the stability regions persist for large delays: Stability boundaries are delay dependent, boundaries are formed by an upper torus bifurcation curve together with two torus bifurcation curves that emanate from Hopf-Hopf points, and there are regions of multistability.

III. THEORY

In this section, we develop approximate solutions of Eq. (3) that are valid not only for large delays, but also for providing a good description of the short delay regime (modes with $k = 1, 2, \dots$). The main assumption made is that the bandpass filter is narrow band such that μ can be considered a small parameter.

The idea is to look for a spectrally pure periodic approximate solution to Eq. (3) of the form

$$x_0(t) = \mathcal{A} \cos(\omega t), \quad (5)$$

and to determine both when such a solution exists as well as the behavior of first order corrections. The first order corrections are split into two parts based on their spectrum: (1) contributions \hat{x}_1 due to higher harmonics, i.e., solutions with frequencies $n\omega$ for integer n with $n > 1$, and (2) contributions x_1 that have other and potentially incommensurate frequencies ω_1 . The higher harmonics will lead to periodic signals that are no longer spectrally pure. Contributions from incommensurate frequencies will lead to quasiperiodic solutions associated with a torus bifurcation.

Accordingly, to first order, we write the approximate solution as

$$x \approx x_0 + \hat{x}_1 + x_1, \quad (6)$$

with the assumption that the corrections \hat{x}_1 and x_1 are small compared to x_0 . The nonlinearity in Eq. (4) can then be expanded to first order,

$$F[x_0^\tau + (\hat{x}_1^\tau + x_1^\tau)] \approx F[x_0^\tau] + F'[x_0^\tau](\hat{x}_1^\tau + x_1^\tau), \quad (7)$$

where F' denotes the first derivative. Since the argument $x_0^\tau = x_0(t - \tau)$ of the nonlinearity is an even periodic function with respect to the delayed time $t - \tau$ [see Eq. (5)], the nonlinearity can be written in terms of a cosine Fourier series. For example, we may write the first term on the right-hand side of Eq. (7) as

$$F[x_0^\tau] = \sum_{n=0}^{\infty} C_n \cos(n\omega[t - \tau]), \quad (8)$$

with the Fourier coefficients C_n given in the Appendix.

We note that constant terms in the Fourier series of F do not contribute because only the time derivative of F appears in Eq. (3). Of the oscillating terms in the expansion of $F[x_0^\tau]$, the ω term may be presumed to be largest for reasons of self-consistency; one expects that the large amplitude solution x_0 has a frequency ω close to the filter's center frequency, whereas higher-harmonic terms are smaller due to the suppression by the filter.

In our solution approach of Eq. (3), we therefore order contributions as follows: The dominant zeroth order approximate solution x_0 is paired with the dominant C_1 term in Eq. (8), yielding

$$\ddot{x}_0 + \mu\dot{x}_0 + x_0 = \mu\gamma \frac{C_1}{\mathcal{A}} \dot{x}_0^\tau, \quad (9)$$

where we used the identity $\cos(\omega[t - \tau]) = x_0^\tau/\mathcal{A}$. This equation implicitly determines the amplitude \mathcal{A} and frequency ω of the dominant solution x_0 in Eq. (5).

To next order, the higher-harmonics correction \hat{x}_1 is paired with the higher-harmonic expansion coefficients C_n ($n > 1$) of $F[x_0^\tau]$ in Eq. (8), yielding

$$\ddot{\hat{x}}_1 + \mu\dot{\hat{x}}_1 + \hat{x}_1 = -\mu\gamma \sum_{n=2}^{\infty} n\omega C_n \sin(n\omega[t - \tau]). \quad (10)$$

This equation expresses the fact that the nonlinearity shifts power from the frequency ω (the x_0 solution) to higher-harmonic frequencies $n\omega$ (the \hat{x}_1 correction). In principle, there is also a contribution to frequency $n\omega$ of \hat{x}_1 from mixing of $m\omega$ components of \hat{x}_1 ($m \neq n$) with the main signal x_0 as expressed in the $F'[x_0^\tau]\hat{x}_1^\tau$ term in Eq. (7). We assume that this is a higher order effect that can be neglected.

Finally, the x_1 correction at nonharmonic frequencies satisfies an equation that is obtained by pairing x_1 and the mixture of x_0 and x_1 as expressed by the $F'[x_0^\tau]x_1^\tau$ term in Eq. (7), yielding

$$\ddot{x}_1 + \mu\dot{x}_1 + x_1 = \mu\gamma \frac{d}{dt} [F'[x_0^\tau]x_1^\tau]. \quad (11)$$

This equation is a linear second order delay differential equation with time-varying coefficients. It determines the stability of the periodic solution x_0 ; x_0 is stable (unstable) if the trivial solution $x_1 = 0$ of Eq. (11) is stable (unstable).

We have separated the nonlinear DDE (3) into three linear differential equations: Eqs. (9), (10), and (11). We solve them in turn.

A. Sinusoidal periodic solution

The dominant periodic solution x_0 satisfies Eq. (9). After substituting the solution ansatz Eq. (5) into the DDE (9), inserting the Fourier coefficient C_1 as given by Eq. (A3), and separately equating the $\cos(\omega t)$ and $\sin(\omega t)$ terms, we find

$$1 = \gamma_{\text{eff}} \cos(\omega\tau) \frac{J_1(2\mathcal{A})}{\mathcal{A}}, \quad (12a)$$

$$\omega^{-1} - \omega = \mu \gamma_{\text{eff}} \sin(\omega\tau) \frac{J_1(2\mathcal{A})}{\mathcal{A}}, \quad (12b)$$

where J_k denotes the Bessel function of the first kind and we have defined the effective feedback-gain parameter,

$$\gamma_{\text{eff}} = -\gamma \sin(2\phi). \quad (13)$$

For all our results, γ_{eff} is the relevant parameter with ϕ just rescaling the gain. This holds as long as $\sin(2\phi)$ is sufficiently large. In contrast, if $\sin(2\phi) \approx 0$, then the linear term in the Taylor expansion of the nonlinearity $F[x]$ becomes negligible compared to the quadratic term, invalidating our approximation scheme. We set $\phi = -\pi/4$ in both numerics and experiment in which case $\gamma_{\text{eff}} = \gamma$.

Equations (12a) and (12b) determine the angular-frequency ω because they imply

$$\omega^{-1} - \omega = \mu \tan(\omega\tau). \quad (14)$$

To this order of approximation, the angular frequency is independent of the oscillation amplitude and is determined solely by the filter through μ and by the delay τ . With ω at hand, the amplitude \mathcal{A} is determined by Eq. (12a).

The solutions ω of the transcendental Eq. (14) correspond to potential delay oscillation modes, but for any given feedback-gain γ_{eff} only a finite number of modes also satisfy Eq. (12a) with a positive amplitude \mathcal{A} . Indeed, it has been shown [24] that periodic solutions only exist if γ_{eff} has a magnitude larger than one. As an example, consider the k th delay oscillation mode for the special case of integer delay $\tau = 2\pi k$ (with k as a positive integer). Then the mode frequency is $\omega = 1$, and one finds from Eq. (12a), after expanding the Bessel function for small argument \mathcal{A} , that \mathcal{A} needs to satisfy

$$\frac{\mathcal{A}}{\sqrt{2}} \approx \sqrt{1 - \frac{1}{\gamma_{\text{eff}}}}. \quad (15)$$

Physically relevant solutions with a positive real amplitude \mathcal{A} exist only if $\gamma_{\text{eff}} > 1$.

B. Harmonics

The higher-harmonic first order correction \hat{x}_1 is easily computed from Eq. (10), which is a damped harmonic oscillator equation with harmonic drive terms. Explicitly, we may write Eq. (10) as

$$\ddot{\hat{x}}_1 + \mu \dot{\hat{x}}_1 + \hat{x}_1 = \sum_{n=2}^{\infty} [a_n \sin(n\omega t) + b_n \cos(n\omega t)]. \quad (16)$$

with coefficients,

$$a_n = n\omega\mu\gamma_{\text{eff}} \cos(n\omega\tau) \Phi_n J_n(2\mathcal{A}), \quad (17a)$$

$$b_n = -n\omega\mu\gamma_{\text{eff}} \sin(n\omega\tau) \Phi_n J_n(2\mathcal{A}), \quad (17b)$$

where the factor Φ_n stands for

$$\Phi_n = \begin{cases} (-1)^{(n+1)/2}, & n = 3, 5, \dots, \\ (-1)^{n/2} \cot[2\phi], & n = 2, 4, 6, \dots \end{cases} \quad (18)$$

Integration gives the solution,

$$\hat{x}_1 = \sum_{n=2}^{\infty} [c_n \cos(n\omega t) + s_n \sin(n\omega t)]. \quad (19)$$

The coefficients in Eq. (19) are

$$c_n = \frac{b_n + a_n n \mu \omega - b_n n^2 \omega^2}{1 + n^2(-2 + \mu^2)\omega^2 + n^4 \omega^4} \approx \frac{b_n}{1 - n^2 \omega^2}, \quad (20a)$$

$$s_n = \frac{a_n - b_n n \mu \omega - a_n n^2 \omega^2}{1 + n^2(-2 + \mu^2)\omega^2 + n^4 \omega^4} \approx \frac{a_n}{1 - n^2 \omega^2}. \quad (20b)$$

The approximation in Eq. (20) is due to the assumption that $\mu \ll 1$.

The harmonics are generated because the nonlinearity in the time-delay-feedback loop shifts power from the dominant solution to its higher-harmonic frequencies. The amplitude of the harmonics scales approximately as $\mu \gamma_{\text{eff}} J_n(2\mathcal{A})/(n\omega)$ for large n , i.e., the amplitudes fall off as $1/n$ and decrease as the filter bandwidth is narrowed ($\mu \rightarrow 0$). Noting that $J_n(2\mathcal{A}) \approx \mathcal{A}^n/n!$ for small \mathcal{A} , i.e., close to oscillation onset, we find that the harmonics are negligibly small and the signal is of high spectral purity. However, as the oscillation amplitude \mathcal{A} of the dominant solution grows with increasing feedback strength, the higher-harmonic frequency terms noticeably distort the sinusoidal solutions as shown in Fig. 4.

C. Stability of periodic solutions

The numerical results of Sec. II suggest that the periodic oscillations lose stability in torus bifurcations, i.e., Andronov-Hopf bifurcations of the amplitudes that lead, generically, to quasiperiodic oscillations. In terms of our theory, a change in stability of the periodic solution x_0 corresponds to a loss of stability of the steady-state solution of Eq. (11). Since Eq. (11) is a linear DDE with periodic coefficients, Floquet theory can be used to determine stability, but such analysis requires numeric computations [25,26]. Instead, we will utilize the fact that the narrow bandpass filter suppresses solutions with frequencies away from the filter's center frequency to reduce the problem to a linear DDE with constant coefficients for which the stability analysis is straightforward.

Due to narrow-band filtering, the x_1 perturbation has most of its power close to the frequency ω and, therefore, we write the perturbation x_1 as

$$x_1 = R(t) \cos(\omega t) - T(t) \sin(\omega t), \quad (21)$$

where we presume that the in-phase amplitude R (radial perturbation) and out-of-phase amplitude T (tangential perturbation) are small and vary slowly, i.e., with frequencies less than $\omega \approx 1$.

Our approach is to expand the right-hand side of Eq. (11) in a Fourier series and to only retain terms that oscillate with frequencies close to ω . That is, this step mirrors the approach that gave rise to the equation for x_0 [Eq. (9)]. We obtain [see Eq. (A6) in the Appendix]

$$\ddot{x}_1 + \mu \dot{x}_1 + x_1 = \mu \gamma_{\text{eff}} \frac{d}{dt} [c_R R^\tau \cos(\omega[t - \tau]) - c_T T^\tau \sin(\omega[t - \tau])], \quad (22)$$

with the \mathcal{A} -dependent coefficients c_R and c_T given by Eq. (A7). Taking advantage of the smallness of μ and the slow variation of R and T , we may drop terms \dot{R} and \dot{T} and terms $\mu \dot{R}$ and $\mu \dot{T}$ (slowly varying envelope approximation). It also follows that one may equate separately the $\cos(\omega t)$ and $\sin(\omega t)$ terms because R and T do not change significantly over one period. After some algebra and use of Eqs. (14) and (A9), we obtain a linear DDE with constant coefficients,

$$\dot{\mathbf{z}}(t) = \mathbf{A}\mathbf{z}(t) + \mathbf{B}\mathbf{z}(t - \tau). \quad (23)$$

Here, $\mathbf{z} = [T, R]^\top$ is a two-dimensional column vector, and the constant matrices are

$$\mathbf{A} = -\frac{\mu}{2} \begin{pmatrix} 1 & -\tan(\omega\tau) \\ \tan(\omega\tau) & 1 \end{pmatrix}, \quad (24a)$$

$$\mathbf{B} = -\frac{\mu}{2} \begin{pmatrix} -1 & \frac{c_R}{c_T} \tan(\omega\tau) \\ -\tan(\omega\tau) & -\frac{c_R}{c_T} \end{pmatrix}. \quad (24b)$$

The stability of the steady state of Eq. (23) is determined by the complex-valued spectrum of eigenvalues Λ that are the roots of the characteristic equation,

$$\det(\Lambda \mathbf{I} - \mathbf{A} - \mathbf{B}e^{-\Lambda\tau}) = 0, \quad (25)$$

where \mathbf{I} is the identity matrix. The steady state is stable if all (infinitely many) roots have negative real parts. Starting with parameters for which the steady state is stable, a destabilizing bifurcation occurs if roots cross the imaginary axis as parameters of the system are varied.

For the stability analysis we consider μ fixed, leaving two bifurcation parameters: the feedback delay τ and the effective feedback-gain γ_{eff} . For notational convenience we introduce

$$g_1 = -\frac{\mu\tau}{2}, \quad g_2 = -\frac{\mu\tau}{2} [1 + \tan(\omega\tau)^2]. \quad (26)$$

These quantities depend on the delay τ but are independent of γ_{eff} . The dependence on the effective feedback-gain γ_{eff} arises through the amplitude \mathcal{A} of the zeroth order solution x_0 [see Eq. (12a)] and is encoded by α , defined as

$$\alpha = \left(1 + \frac{c_R}{c_T}\right) = \frac{2\mathcal{A}J_0(2\mathcal{A})}{J_1(2\mathcal{A})}. \quad (27)$$

With these definitions, the characteristic equation (25) becomes

$$0 = (\Lambda\tau)^2 - 2g_1\Lambda\tau + g_1\alpha\Lambda\tau e^{-\Lambda\tau} + g_1g_2(1 - e^{-2\Lambda\tau} - \alpha e^{-\Lambda\tau} + \alpha e^{-2\Lambda\tau}). \quad (28)$$

We note that $\Lambda = 0$ is a solution of Eq. (28) for any choice of parameter values. The corresponding eigenvector is $\mathbf{z} = [1, 0]^\top$ (for positive amplitudes \mathcal{A}), implying that $x_1 =$

$-T_0 \sin(\omega t)$ for some constant T_0 such that $x_0 + x_1$ is simply a phase shifted periodic solution. In other words, the $\Lambda = 0$ solution of Eq. (28) does not indicate a bifurcation but is due to the time-shift invariance of Eq. (3).

To find Andronov-Hopf bifurcations of the steady-state $\mathbf{z} = 0$, we set $\Lambda = i\omega_1$, separate real and imaginary parts, and solve for α to obtain

$$\alpha = \frac{(\omega_1\tau)^2/g_1 - g_2 + g_2 \cos(2\omega_1\tau)}{\omega_1\tau \sin(\omega_1\tau) - g_2 \cos(\omega_1\tau) + g_2 \cos(2\omega_1\tau)}, \quad (29a)$$

$$\alpha = \frac{2\omega_1\tau - g_2 \sin(2\omega_1\tau)}{\omega_1\tau \cos(\omega_1\tau) + g_2 \sin(\omega_1\tau) - g_2 \sin(2\omega_1\tau)}. \quad (29b)$$

Eliminating α from Eqs. (29a) and (29b) yields a transcendental equation for the frequency ω_1 of $R(t)$ and $T(t)$ that only depends on μ and τ and is independent of the feedback-gain γ_{eff} . That is, the feedback delay alone determines both the frequency ω of the periodic oscillation and the secondary frequency ω_1 that arises in the torus bifurcation.

Numerical root finding allows one to determine ω_1 for a given feedback delay τ and then calculate the corresponding feedback-gain γ_{eff} using Eq. (12a) after first utilizing Eq. (29a) to find α and Eq. (27) to obtain \mathcal{A} . Among the infinitely many positive roots ω_1 of the transcendental equation, the lowest frequencies that give rise to positive γ_{eff} are the frequencies of interest. The solutions thus obtained are torus-bifurcation curves $\gamma_{\text{eff}}(\tau)$ that bound regions of stable oscillations. The result is shown in Fig. 5 and discussed in Sec. V.

IV. EXPERIMENTAL SETUP

The theory depends on frequency ratios only. In light of this, we chose to perform experiments at low frequencies for ease of implementation.

In the experiment, schematically shown in Fig. 1, continuous-wave light from a 1554 nm fiber-coupled semiconductor laser passes through a polarization controller and is injected into a JDSU Z5 LiNbO₃ Mach-Zehnder modulator. The optical power P transmitted through the modulator is a nonlinear function of the applied voltages $P_{\text{out}}/P_{\text{in}} \sim \cos^2[x(t) + \phi]$, where $x(t) = \pi V(t)/(2V_\pi)$ with $V_\pi = 2.7$ V is the dimensionless variable corresponding to the time-varying voltage $V(t)$ coming from the feedback loop and ϕ is a dimensionless parameter corresponding to a constant bias voltage. For all data shown in this paper, $\phi = -\pi/4$ (positive feedback). The optical output of the nonlinearity is detected and converted to an electrical signal by a ThorLabs PDA20CS InGaAs photodetector. The adjustable delay is achieved through a Symetrix 402 delay, which delays audio-frequency signals by up to 885 ms with fine adjustable delay steps of approximately 0.88 ms. The audio-delay output is fed into an amplifier controlled by a digital potentiometer that ensures precise control of the loop gain. The signal is then passed through a bandpass filter with center-frequency $\Omega_0 = 2\pi \times 8.38$ Hz and bandwidth $\Delta\Omega = 2\pi \times 1.86$ Hz. Finally, the filtered output is added to a dc bias voltage that sets ϕ , and the sum signal is fed into the dc input port of the Mach-Zehnder modulator.

The filter transfer function as well as the absolute values of the total loop delay and gain are measured in an open

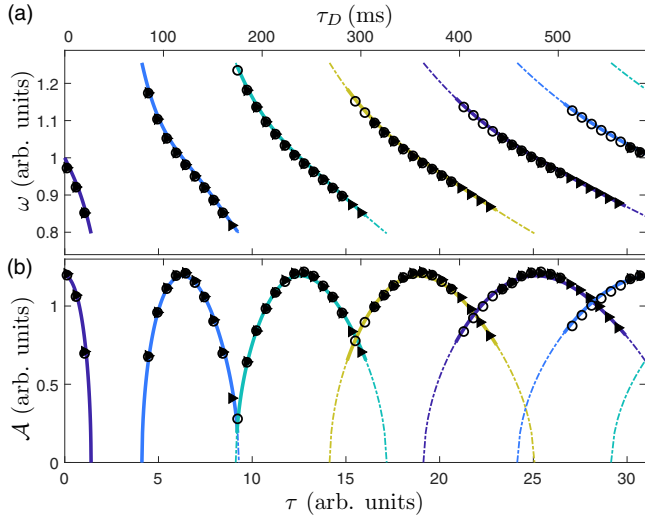


FIG. 3. Sinusoidal periodic solutions: (a) frequency, (b) amplitude for $\gamma_{\text{eff}} = 2.28$ (dotted horizontal line in Fig. 2). Data: increasing delay (solid triangles) and decreasing delay (open circles). Theory: stable (solid lines) and unstable (dashed-dotted lines) periodic solutions $x_0(t)$. Horizontal axis: both the dimensionless delay τ and the corresponding measured delay τ_D are given.

loop configuration. Thus, all parameters are known, and no fits are performed when comparing the closed loop dynamics generated by the experiment with theory.

V. RESULTS

The results in Fig. 3 are obtained by fixing the effective feedback gain and varying the delay thereby scanning along the dotted horizontal line in Fig. 2(a). We find good quantitative agreement between measurements and theoretical predictions both in terms of oscillation frequencies and amplitudes. The close match of the oscillation amplitudes is especially noteworthy because it confirms the sufficiency of the two-pole bandpass filter model; details of filter roll-off behavior far from the filter's center frequency has a negligible effect on the dynamics.

It is seen in Fig. 3(a) that the mode frequency of the observed sinusoidal signal decreases for each delay oscillation mode as the delay increases. Approximately, the period increases linearly with delay, $T \approx \tau/k$ for integer k . As shown in Fig. 3(b), the amplitudes are maximum for delays that lead to oscillation frequencies near the maximum transmission frequency of the bandpass filter ($\omega = 1$, corresponding to 8.38 Hz) but decrease for larger delays because the mode frequency shifts toward the low-frequency end of the filter. As the delay is increased further, the next harmonic mode has a higher net feedback loop gain, and a mode jump occurs.

Figure 3 clearly shows that stable single-frequency oscillation modes coexist for certain delays. For example, the larger period (lower-frequency) $\tau/3$ mode and smaller period (higher-frequency) $\tau/4$ mode coexist for delays $\tau \in [21, 23]$. Experimentally, the two modes are accessed by entering the delay interval of multistability by either increasing the delay (triangles, $\tau/3$ mode) or decreasing the delay (open circles, $\tau/4$ mode).

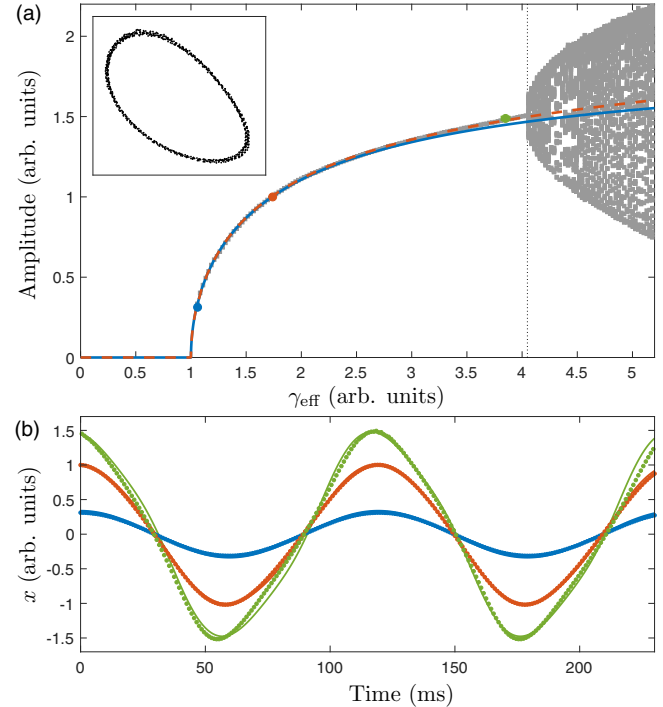


FIG. 4. Periodic solutions and higher harmonics for a delay $\tau = 6.27$, corresponding to 119 ms [dotted vertical lines in Figs. 2(a) and 5]. (a) Amplitude of periodic solution x_0 (solid blue line) and $x_0 + \hat{x}_1$ (dashed red line) and local maxima of experimental time series (gray squares and colored circles). Theoretical torus bifurcation value (dotted line at $\gamma_{\text{eff}}^{\text{tor}} = 4.05$). The inset: Poincaré section of delay-embedded experimental time series at $\gamma_{\text{eff}} = 4.24$. (b) Experimental time series (circles) and $x_0 + \hat{x}_1$ (solid lines) for $\gamma_{\text{eff}} = 1.06, 1.74, \text{ and } 3.85$, corresponding to the circles in panel (a).

Figure 4 displays results obtained by fixing the feedback delay and increasing the feedback gain thereby scanning along the dotted vertical line in Figs. 2(a) and 5. Experimental observations are in remarkable agreement with theoretical

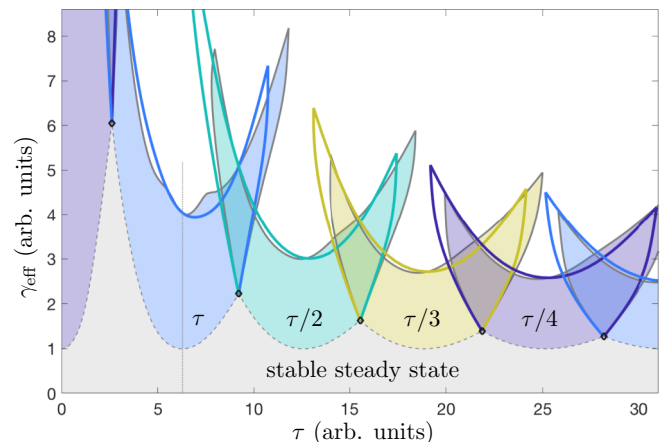


FIG. 5. Stability regions of periodic oscillations from theory and numerics. Numerics: color shaded regions with thick gray solid line boundaries. Theory: unshaded region bounded by thick colored solid lines. Dotted vertical line: $\tau = 6.27$.

results; both the measured amplitudes of the stable periodic solutions [Fig. 4(a)] and the waveform shape [Fig. 4(b)] are visually indistinguishable from the theoretical predictions with the exception of the large feedback-gain time series in Fig. 4(b) (green curve, $\gamma_{\text{eff}} = 3.85$).

The effect of the higher-harmonic correction on the oscillation amplitude is small as seen by the near coincidence of the solid blue line (no correction) and dashed red line (with correction) prediction that are shown in Fig. 4(a). The higher-harmonic correction does, however, lead to a noticeable shark-fin like distortion of the signal as the feedback gain is increased as seen in Fig. 4(b).

The data shown in gray in Fig. 4(a) are the local maxima of the recorded time series. The creation of stable periodic oscillations in a supercritical Andronov-Hopf bifurcation at $\gamma_{\text{eff}} \approx 1$ is clearly seen as is the destabilization of the periodic solution in a secondary supercritical Hopf bifurcation (torus bifurcation) at $\gamma_{\text{eff}}^{\text{tor}} \approx 4.05 \pm 0.03$. Our experimental results confirm the creation of stable torus attractors at the upper threshold. As an example, we show in the inset of Fig. 4(a) the Poincaré section of a torus attractor. The plot is obtained by delay embedding [27] the experimental time series in a three-dimensional space and then plotting the one-way intersections of the system trajectory with a two-dimensional Poincaré plane. The result is the closed curve shown, demonstrating that the attractor is indeed a torus. The width of the curve is due to measurement noise.

The torus bifurcation value found numerically is $\gamma_{\text{eff}}^{\text{tor}} = 4.04$, whereas the theoretical result is $\gamma_{\text{eff}}^{\text{tor}} \approx 4.05$ [see the dotted line in Fig. 4(a)]. Both values agree with the experimentally determined threshold of $\gamma_{\text{eff}}^{\text{tor}} \approx 4.05 \pm 0.03$ within experimental uncertainties.

One does not necessarily expect a first order perturbation theory to yield such quantitatively accurate predictions and indeed as shown in Fig. 5, whereas the agreement between torus bifurcation curves determined numerically and theoretically is excellent for a delay value of $\tau = 6.27$, there are noticeable differences for other delay values. Nevertheless, the theory correctly reproduces the general structure of bifurcations. It not only finds the delay-dependent upper gain threshold, but also finds the torus bifurcation curves that emanate from the Hopf-Hopf bifurcation points.

VI. DISCUSSION

In this paper we show that OEOs with a single time-delayed narrow-band feedback loop can produce stable periodic solutions if signal amplitudes are small. The presented theory provides approximate analytic periodic solutions and their stability boundaries. Our analytical predictions agree closely with both numerical results and experiments.

Of note is the significant delay dependence of the stability boundaries as well as the existence of regions of multistability. Not only do stable periodic solutions coexist, but also stable quasiperiodic solutions may coexist with stable periodic oscillations, depending on the chosen parameters.

We note that the critical value of $\gamma_{\text{eff}}^{\text{tor}} \approx 2.31$ obtained by Chembo *et al.* [16] is recovered from our theory by considering the spectrum of Eq. (23) in the limit of large delays [28]. This asymptotic value provides a good estimate

of the upper stability threshold's minimum value already for medium delays, such as the $T \approx \tau/16$ delay mode whose stability region is depicted at the center of Fig. 2(b).

Independent of the chosen delay, one finds that sinusoidal signals become distorted as the feedback gain is increased and the signal amplitude grows, resulting in additional harmonic frequencies in the signal's spectrum. Upon further increase in the feedback gain, the periodic oscillations undergo a torus bifurcation. Although the torus bifurcation will give rise to quasiperiodic oscillations generically, we do expect that frequency locking regions (Arnold tongues) exist but have not attempted to locate these regions. We also note that the torus bifurcation curves that limit the parameter region of a stable τ/k oscillation mode intersect. It would be interesting to understand what the dynamics are for parameters close to those intersections.

Finally, we would like to emphasize that the stability analysis in this paper is purely local. The local theory correctly predicts the global dynamics at $\tau = 6.27$, shown in Fig. 4(a). There, the torus bifurcation is supercritical and the periodic solutions at gain values smaller than the upper stability threshold appear to be either globally attracting or, at least, have a large basin because they are the only solutions observed in experiment. Yet, we have no reason to expect that the same is true for all delays.

ACKNOWLEDGMENTS

This paper was supported, in part, by the Delord-Mockett Fund, the Borders Physics Research Fellowship, and the Reed College Science Research Fellowship.

APPENDIX: JACOBI-ANGER EXPANSION OF THE NONLINEARITY

The nonlinearity in Eq. (4) with the dominant solution [Eq. (5)] as an argument is given by

$$F[x_0^\tau] = \frac{1}{2} + \frac{1}{2} \cos[2\mathcal{A} \cos(\omega[t - \tau])] \cos(2\phi) - \frac{1}{2} \sin[2\mathcal{A} \cos(\omega[t - \tau])] \sin(2\phi), \quad (\text{A1})$$

and may be written as a Fourier series,

$$F[x_0^\tau] = \sum_{n=0}^{\infty} C_n \cos(n\omega[t - \tau]) \quad (\text{A2})$$

by utilizing the Jacobi-Anger expansion,

$$\cos(z \cos \theta) = J_0(z) + 2 \sum_{n=1}^{\infty} (-1)^n J_{2n}(z) \cos(2n\theta),$$

$$\sin(z \cos \theta) = -2 \sum_{n=1}^{\infty} (-1)^n J_{2n-1}(z) \cos[(2n-1)\theta],$$

where J_k is the k th order Bessel function of the first kind. We find the Fourier coefficients to be

$$C_0 = \frac{1}{2} + \frac{1}{2} J_0(2\mathcal{A}) \cos(2\phi), \quad (\text{A3a})$$

$$C_n = \begin{cases} (-1)^{(n+1)/2} J_n(2\mathcal{A}) \sin(2\phi), & n = 1, 3, \dots, \\ (-1)^{n/2} J_n(2\mathcal{A}) \cos(2\phi), & n = 2, 4, \dots \end{cases} \quad (\text{A3b})$$

We also need the term $F'[x_0^\tau]x_1^\tau$ with x_0 given by Eq. (5) and x_1 given by Eq. (21). The Fourier series of the first derivative of the nonlinearity is again obtained via the Jacobi-Anger expansion,

$$F'[x_0^\tau] = -\sin(2x_0[t - \tau] + 2\phi), \quad (\text{A4a})$$

$$= \sum_{n=0}^{\infty} \hat{C}_n \cos(n\omega[t - \tau]) \quad (\text{A4b})$$

with coefficients,

$$\hat{C}_0 = -J_0(2\mathcal{A}) \sin(2\phi), \quad (\text{A5a})$$

$$\hat{C}_n = \begin{cases} (-1)^{(n+1)/2} 2J_n(2\mathcal{A}) \cos(2\phi), & n = 1, 3, \dots, \\ -(-1)^{n/2} 2J_n(2\mathcal{A}) \sin(2\phi), & n = 2, 4, \dots \end{cases} \quad (\text{A5b})$$

We are looking for a solution x_1 with frequency close to ω and assume slowly varying R and T . Accordingly, the most relevant terms in the Fourier series of $F'[x_0^\tau]x_1^\tau$ are terms with frequencies close to ω . Contributions at frequency ω arise due to two terms in the Fourier series (A4b): the constant term (coefficient \hat{C}_0) and the 2ω term (coefficient \hat{C}_2). Neglecting both slowly varying as well as high-frequency

terms of $F'[x_0^\tau]x_1^\tau$, we find that

$$\gamma F'[x_0^\tau]x_1^\tau \approx \gamma_{\text{eff}} c_R R^\tau \cos(\omega[t - \tau]) - \gamma_{\text{eff}} c_T T^\tau \sin(\omega[t - \tau]), \quad (\text{A6})$$

where we made use of the definition of γ_{eff} given by Eq. (13) and introduced c_R and c_T , which are functions of the amplitude \mathcal{A} of x_0 ,

$$c_R = J_0(2\mathcal{A}) - J_2(2\mathcal{A}) = \frac{dJ_1(2\mathcal{A})}{d\mathcal{A}}, \quad (\text{A7a})$$

$$c_T = J_0(2\mathcal{A}) + J_2(2\mathcal{A}) = \frac{J_1(2\mathcal{A})}{\mathcal{A}}. \quad (\text{A7b})$$

We further rewrite Eq. (A6) by noting that Eq. (12a) implies

$$\gamma_{\text{eff}} \cos(\omega\tau) = \frac{1}{J_1(2\mathcal{A})/\mathcal{A}} = \frac{1}{c_T}, \quad (\text{A8})$$

which, upon expanding the trigonometric functions, yields

$$\gamma F'[x_0^\tau]x_1^\tau \approx \left[\frac{c_R}{c_T} R^\tau + T^\tau \tan(\omega\tau) \right] \cos(\omega t) + \left[\frac{c_R}{c_T} \tan(\omega\tau) R^\tau - T^\tau \right] \sin(\omega t). \quad (\text{A9})$$

-
- [1] G. D. VanWiggeren and R. Roy, *Science* **279**, 1198 (1998).
- [2] A. Argyris, D. Syvridis, L. Larger, V. Annovazzi-Lodi, P. Colet, I. Fischer, J. Garcia-Ojalvo, C. R. Mirasso, L. Pesquera, and K. A. Shore, *Nature (London)* **438**, 343 (2005).
- [3] A. Uchida, K. Amano, M. Inoue, K. Hirano, S. Naito, H. Someya, I. Oowada, T. Kurashige, M. Shiki, S. Yoshimori *et al.*, *Nat. Photonics* **2**, 728 (2008).
- [4] I. Kanter, Y. Aviad, I. Reidler, E. Cohen, and M. Rosenbluh, *Nat. Photonics* **4**, 58 (2009).
- [5] L. Appeltant, M. C. Soriano, G. Van der Sande, J. Danckaert, S. Massar, J. Dambre, B. Schrauwen, C. R. Mirasso, and I. Fischer, *Nat. Commun.* **2**, 468 (2011).
- [6] L. Larger, M. C. Soriano, D. Brunner, L. Appeltant, J. M. Gutierrez, L. Pesquera, C. R. Mirasso, and I. Fischer, *Opt. Express* **20**, 3241 (2012).
- [7] Y. Paquot, F. Duport, A. Smerieri, J. Dambre, B. Schrauwen, M. Haelterman, and S. Massar, *Sci. Rep.* **2**, 287 (2012).
- [8] X. S. Yao and L. Maleki, *J. Opt. Soc. Am. B* **13**, 1725 (1996).
- [9] L. Maleki, *Nat. Photonics* **5**, 728 (2011).
- [10] T. Erneux, L. Larger, M. W. Lee, and J. P. Goedgebuer, *Physica D* **194**, 49 (2004).
- [11] T. Erneux, *Applied Delay Differential Equations*, Surveys and Tutorials in the Applied Mathematical Sciences Vol. 3 (Springer-Verlag, New York, 2009).
- [12] M. Peil, M. Jacquot, Y. K. Chembo, L. Larger, and T. Erneux, *Phys. Rev. E* **79**, 026208 (2009).
- [13] K. E. Callan, L. Illing, Z. Gao, D. J. Gauthier, and E. Schöll, *Phys. Rev. Lett.* **104**, 113901 (2010).
- [14] L. Larger and J. M. Dudley, *Nature (London)* **465**, 41 (2010).
- [15] L. Illing, C. D. Panda, and L. Shareshian, *Phys. Rev. E* **84**, 016213 (2011).
- [16] Y. K. Chembo, L. Larger, and P. Colet, *IEEE J. Quantum Electron.* **44**, 858 (2008).
- [17] Y. K. Chembo, L. Larger, H. Tavernier, R. Bendoula, E. Rubiola, and P. Colet, *Opt. Lett.* **32**, 2571 (2007).
- [18] H. D. I. Abarbanel, M. B. Kennel, L. Illing, S. Tang, H. F. Chen, and J. M. Liu, *IEEE J. Quantum. Electron.* **37**, 1301 (2001).
- [19] D. Pieroux, T. Erneux, B. Haegeman, K. Engelborghs, and D. Roose, *Phys. Rev. Lett.* **87**, 193901 (2001).
- [20] J. M. Saucedo Solorio, D. W. Sukow, D. R. Hicks, and A. Gavrielides, *Opt. Commun.* **214**, 327 (2002).
- [21] L. Illing and D. J. Gauthier, *Chaos* **16**, 033119 (2006).
- [22] K. Engelborghs, T. Luzyanina, and D. Roose, *ACM Trans. Math. Software* **28**, 1 (2002).
- [23] J. Sieber, K. Engelborghs, T. Luzyanina, G. Samaey, and D. Roose, *arXiv:1406.7144*.
- [24] L. Illing and D. J. Gauthier, *Physica D* **210**, 180 (2005).
- [25] O. Diekmann, S. Gils, S. van, Lunel, and H.-O. Walther, *Delay Equations: Functional-, Complex-, and Nonlinear Analysis* (Springer-Verlag, New York, 1995).
- [26] X. Long, T. Insperger, and B. Balachandran, in *Delay Differential Equations*, edited by D. E. Gilsinn, T. Kalmár-Nagy, and B. Balachandran (Springer, Boston, MA, 2009), pp. 131–153.
- [27] H. D. I. Abarbanel and U. Parlitz, in *Handbook of Time Series Analysis*, edited by B. Schelter, M. Winterhalder, and J. Timmer (Wiley-VCH, Weinheim, 2006), pp. 5–38.
- [28] S. Yanchuk, *Math. Meth. Appl. Sci.* **28**, 363 (2004).